Laser modelocking and dual wavelength lasing in silicon

En-Kuang Tien, Xinzhu Sang and Ozdal Boyraz.
Department of Electrical Engineering & Computer Science, University of California, Irvine, Irvine, CA, USA 92697

ABSTRACT

Nonlinear optics in silicon has drawn substantial attention in the recent years. In this research, laser mode-locking and dual wavelength lasing are achieved in a fiber-ring-cavity using an Erbium–doped fiber amplifier (EDFA) as a gain medium and a 1.7cm long silicon-on-insular waveguide as pulse compressor, a mode-locker and a Raman gain media. We show that the transient behavior of two photon absorption (TPA) and TPA induced free carrier absorption can be used for pulse compression and laser modelocking in the silicon waveguide inside the laser cavity. The proposed technique takes advantage of spontaneous generation of free carriers and the slow recombination time, >17ns, to attenuate the trailing edge of the time varying signals passing through the waveguide. When a 5μm^2 model area silicon waveguide is placed inside a fiber ring cavity consisting of an EDFA as a gain media and ~50ps modelocked laser pulses are generated at 1540nm. We also observe that the generated short pulses also induce stimulated Raman scattering at 1675nm in the same silicon waveguide. We show that engineering the laser cavity facilitates laser modelocking and dual wavelength laser oscillation at 1540nm and 1675nm. Experimentally we obtain <100ps modelocked pulses at both wavelengths. The average pump threshold power of the Raman laser is measured to be 3.75mW and the Stokes average output power is measured to be 3 μW.

Keywords: Mode-locking, silicon waveguide, ultrafast nonlinear optics, Raman laser,.

1. INTRODUCTION

Because of its possible dense on-chip integration with microelectronics and significant advances in nonlinear effects, silicon photonics has become a rapidly growing field. Due to the high-index contrast between the silicon core and silica cladding, silicon waveguides allow strong optical confinement and large effective nonlinearity, which facilitates low cost chip-scale demonstration of all-optical nonlinear functional devices at relatively low pump powers. In fact, nonlinear photonic phenomena and devices in silicon, such as Raman amplification and lasing [1-4], optical modulation [5-6], wavelength conversion [7-9], all-optical switching [10-12], pulse compression [13-14], control of slow light [15-16] and so on, have been successfully demonstrated. Two-photon absorption (TPA) and TPA-induced free carrier absorption (FCA) are nonlinear losses dominating at high intensities. Because they introduce additional loss, so far they have been considered as detrimental effects in nonlinear photonic silicon devices. However, engineered use of TPA and FCA may increase the capabilities of silicon photonics in different applications [13, 17]. A novel approach to utilize TPA and FCA losses for ultrafast pulse shaping and modelocked pulse generation has been demonstrated. We present a detailed theoretical and experimental investigation on free carrier absorption (FCA) transients and TPA with special emphasis on their effects on self pulse compression. To assess this competition and its effects on the pulse compression, we calculate the temporal behavior of TPA and FCA generated by 10ps to 1000ps wide optical pulses with peak intensities up to 40GW/cm^2. We show that TPA produced at the peak intensity by pulses shorter than 50 ps surpasses the free carrier losses at the trailing edge and hence produces net pulse broadening even at 50nJ pulse energy values (40GW/cm^2 peak intensity). As the pulse energy increases to 500nJ by increasing the pulse width, the losses at the trailing edge dominate and produce 40% pulse compression ($\tau_{out}/\tau_{in} \sim 0.6$). Experimentally, we demonstrate that modelocking by silicon can

Photonic Fiber and Crystal Devices: Advances in Materials and Innovations in Device Applications II, edited by Shizhuo Yin, Ruyan Guo,
Proc. of SPIE Vol. 7056, 70561W, (2008) · 0277-786X/08/$18 · doi: 10.1117/12.794459

produce 60ps optical pulses with 60nJ pulse energy inside the laser cavity, without contributions from group velocity dispersion and self phase modulation induced pulse shaping. Here we also show that created modelocked pulses can stimulate a Raman effect in the same silicon waveguide and provide dual wavelength lasing. Dual-wavelength modelocked laser pulses operating at 1540 nm and 1675 nm are experimentally demonstrated. These results indicate that TPA and other nonlinear effects in silicon, such as Raman and four-wave mixing, can be simultaneously utilized to enhance the functionality of the silicon chip without using an external pump laser. In particular, the proposed technique can provide short pulses at longer wavelengths where short pulse light sources are sparsely available.

2. PRICINPLE AND SIMULATIONS OF PULSE COMPRESSION IN SILICON

Two-photon absorption (TPA) and TPA-induced free carrier absorption (FCA) are two ubiquitous nonlinear effects in silicon for any wavelength between 1.1 μm and 2.2 μm. TPA in silicon is a nonlinear process related to the intensity square. It has higher attenuation at high optical intensities and TPA will contribute to a pulse broadening in silicon. On the other hand, free carrier absorption tends to attenuate the trailing edge of the pulse and it is the pulse shortening mechanism in our system.

The pulse envelope evolution in the presence of optical nonlinearities is conventionally estimated by solving the nonlinear Schrödinger equation [10, 14]:

$$\frac{\partial E(t,z)}{\partial z} = -\frac{1}{2}\left\{ \alpha + \alpha_{FCA}(t,z) + \alpha_{TPA}(t,z) \right\} E(t,z) - i\gamma \left|E(t,z)\right|^2 E(t,z) + i\frac{2\pi}{\lambda}\Delta n(t,z)\, E(t,z) \tag{1}$$

where the parameters *E(t,z)* represent the electric-field, α is the attenuation constants, γ is the effective nonlinearity and Δn is the free carrier induced index change, respectively. The pulse shaping is determined by the nonlinear losses on the right hand side of the equation (1). Among two nonlinear loss terms, the TPA,

$$\alpha_{TPA} = \frac{1}{z}\ln(1+\beta I_0 z) \tag{2}$$

is an intensity dependent and memoryless attenuation following the pulse shape. Here α_{TPA} is the TPA coefficient (0.45 cm/GW at 1550nm [18]), A_{eff} is the effective area of the waveguide and Io is the intensity. However, the FCA,

$$\alpha_{FCA}(z,t) = 1.45\times10^{-17}\left(\frac{\lambda}{1.55}\right)^2 N(z,t)\ \left(\mathrm{cm}^{-1}\right) \tag{3}$$

has memory and is accumulative [13]. For CW signals or time varying signals wider than free carrier recombination time, τ_o, free carrier densities will be stabilized at a local *N(z)* value of: $N(z)=\tau_o \beta I^2(z) / 2h\upsilon$ after $\sim\tau_o$. On the other hand, time varying optical signals with pulse width smaller than τ_o will result in different time dependent local free carrier densities and FCA along the waveguide governed by the equation :

$$\frac{dN(t,z)}{dt} = -\frac{N(t,z)}{\tau_0} + \beta\frac{I^2(t,z)}{2h\upsilon} \tag{4}$$

Fig. 1 illustrates the schematic diagram of pulse propagation in a silicon waveguide where free-carrier losses are significant, and also the amount of free-carrier-induced losses. Upon entering the waveguide the front end of the pulse will be slightly attenuated by TPA and hence the free carriers will start to accumulate wherever the optical energy is present. As a result, the photons entering the waveguide will suffer from the free-carrier losses generated by the earlier photons. This process will lead to attenuation of the trailing edge of the pulse and hence the pulse compression in the time domain, (see Fig. 1(a)). Because of the linear and nonlinear absorption, the free-carrier absorption will be spatially

varying and will be much stronger at the input facet of the silicon waveguide. Fig. 1(b) quantifies the loss and free-carrier accumulation along a 100ps rectangular pulse to give a better understanding of the concept. The results presented here are calculated for a silicon waveguide with 5 μm^2 effective area, similar to the one used in the experiment, for three different peak power values of 100W, 40W and 15W. At the front facet of the waveguide, an optical pulse with 100 W peak power level is expected to create free carriers, the free carrier density increased from 0 to $>10^{19}$ cm^{-3} from beginning time (t=0) to end of the pulse (t=100 ps). As a result, the trailing edge of the pulse is expected to experience 16 cm^{-1} free-carrier-induced loss at that position while the leading edge travels with only TPA loss. The same loss value reduces to ~3 cm^{-1} if the input peak power is reduced to 15W. These results show that dynamic control of free-carrier concentration at a given position can be used for optical signal processing and optical pulse compression.

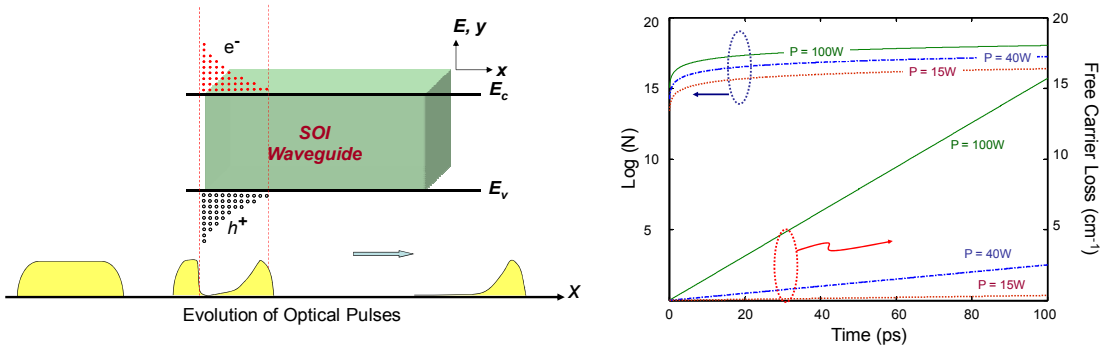

Fig. 1. (a) Schematic description of free-carrier accumulation for pulse compression. A high-intensity optical pulse will leave paint of free carriers behind, which will contribute to pulse attenuation at the trailing edge and hence compression. (b) Temporal variation of free-carrier concentration and losses generated by 100ps optical pulses. The loss difference between the front and end of the pulse can be as high as 16cm^{-1} for optical pulses with 100W peak power values.

We utilize the free-carrier absorption to demonstrate laser modelocking and short pulse generation by using silicon waveguides, which is a three step process. In the first step, an optical modulation is needed to initiate pulsation in the cavity to increase peak power and start free-carrier transients. This modulation can be performed by using the silicon waveguide itself [4, 10-11] or bulk electro-optic modulators. In the second step, this pulse is amplified by a gain medium and then compressed by free carriers. The pulse compression will occur at the leading edge of the pulse by suppressing the trailing edge due to free-carrier absorption. In the third step, recirculation of this pulse helps to form short pulses at the steady state. Conventionally, passively modelocked lasers require saturable absorbers to suppress the low intensity background and initiate oscillation of intensity spikes. The active modelocked lasers, on the other hand, require optical modulators to initiate pulsation at harmonics of the fundamental cavity frequency. In order to create short pulses, the modulation signal has to be short. The free-carrier absorption can alleviate the short pulse modulation requirement if it is used as a pulse shaping mechanism inside the laser cavity. The modulation part of our scheme resembles the active modelocking. However, free-carrier absorption behaves like a saturable absorber on the trailing edge and provides unique pulse shaping method inside the cavity. A numerical case study has been conducted for 400ps electro-optic modulation followed by pulse propagation inside a laser cavity, as depicted in Fig. 2. The silicon waveguide is chosen to be 2 cm long. We use pulse equation (1) to calculate final pulse width after 20 roundtrips. We observe that after 20 cavity roundtrips the pulse width inside the cavity reduces to 20ps. Here the 20 round trips case is chosen for illustration purposes and it is not the steady state value. However, the final pulse width will be a function of the modulation signal and the interplay between TPA and free-carrier loss.

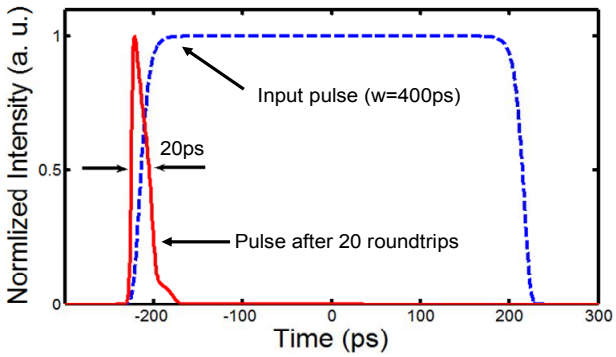

Fig. 2. Simulation results of modelocking by using 400ps modulation signals. A 400ps modulation signal compresses to 20ps after 20 roundtrips inside the cavity.

For pulse shaping, time and space dependent free carrier density, $N(z,t)$, and the nonlinear losses are the utmost important parameters to be determined. Based on the peak intensity and the pulse energy, the nonlinear response of silicon can be divided into two separate regimes in time and in space: TPA dominated regime and FCA dominated regime [19]. Fig. 3 illustrates the calculated outcome of two different regimes for 20ps and 500ps optical pulses with 1 kW peak power (i.e. 20 nJ and 500 nJ pulse energies). The waveguide is set to be 1 cm long with 5 μm^2 effective area and 16ns free carrier lifetime. The fixed 1 kW peak power facilitates the same level of TPA (90%) at the center for comparison, Fig. 3(a). However, FCA generated by 500 nJ pulse is 40x stronger than the FCA generated by 20 ps pulses at the same peak intensity due to difference in number of absorbed photons. We estimate that while 20 nJ pulses are being broadened due to the TPA dominance, 500nJ pulses are being compressed to 350 ps by FCA dominance, Fig 3(b). Here results are presented in normalized time unit, t/τ_{FWHM}, where τ_{FWHM} is the pulse width at the waveguide input, to have better comparisons of output pulses for different input conditions and to have better visualization. The free carrier plasma effect is always present and, unlike FCA and TPA competition, produces a steady linear phase change across the pulse. However, due to the larger free carrier density, high energy pulses experience ~4x larger phase change across the pulse, Fig. 3(b). A blue shifted spectral broadening has been attributed to this phase change when it is combined with self phase modulation, as previously shown [10].

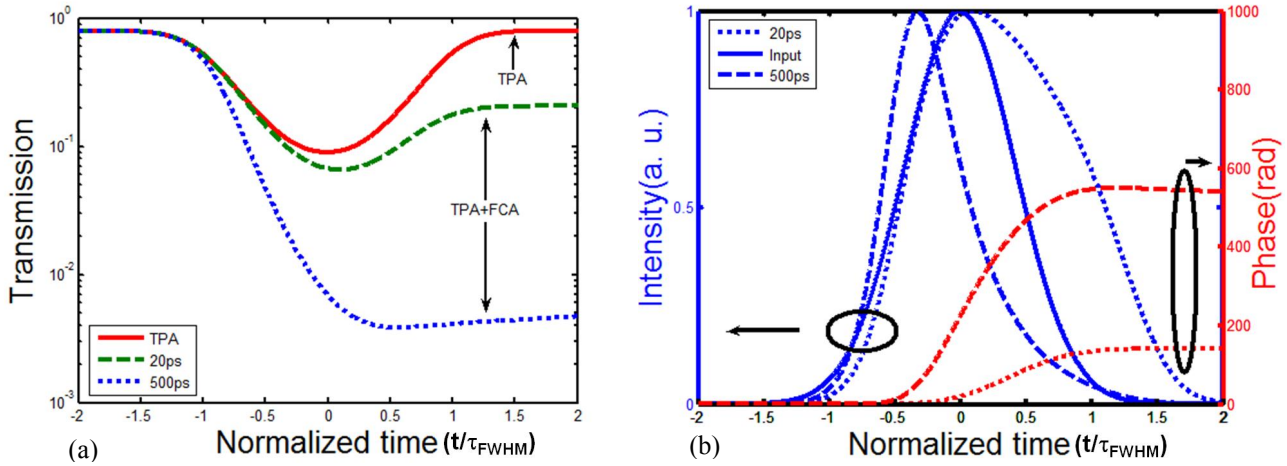

Fig. 3. (a) TPA and free carrier loss profiles of 20 ps and 500 ps wide input pulses. (b) Estimated output pulses and chirp induced by free carrier plasma effect. The font end of both pulses are under TPA dominant nonlinear regime. However, due to excess free carriers, the trailing edge of 500 ps pulse is under FCA dominant nonlinear regime.

The losses presented here represent aggregate attenuation at the end of the waveguide. We expect that the total length of the waveguide, input pulse width and the pulse energy will have prominent influence on the final outcome. Fig. 4(a) illustrates the compression behavior of 10ps to 1000ps optical pulses in a 1cm long silicon waveguide. At low peak powers, < 10^{16} cm^{-3} carriers are generated to facilitate attenuation of the trailing edge and to provide self compression [13]. However, stronger TPA at the center of the pulse dominates at these intensities and induces net pulse broadening at 3dB point. Free carrier dominance is expected at higher intensities. For example, 1ns pulses with 2 GW/cm^2 intensities generate 4×10^{18} cm^{-3} free carriers which dominate over TPA at the center of the pulse and facilitate net self compression. For 500ps and 100ps wide optical pulses, it requires 3 GW/cm^2 (75nJ) and 32 GW/cm^2 (160nJ) to initiate the same type of compression, respectively. For input pulses shorter than 50ps, TPA induced pulse broadening surpasses the self compression even at 40 GW/cm2 and hence net pulse broadening is expected. However, we should note that, simple free carrier density calculations may not be reliable at such a high intensities due to Auger recombination [20]. For instance, as the free carrier density increases from 10^{18} cm^{-3} to 10^{19} cm^{-3} the free carrier lifetime due to Auger effect will reduce from ~1.3 μs to ~20 ns, which is comparable to free carrier lifetime of our waveguides. Fig. 4(b) demonstrates the effect of waveguide length on the pulse compression. For longer waveguides, the front end of the waveguide facilitate FCA dominated nonlinear behavior with >10^{18} cm^{-3} free carriers. The back end, on the other hand, operates in TPA dominated regime and contributes mostly on pulse broadening and loss. Specifically, the free carrier density at the trailing edge of a 100ps pulse is estimated to be ~10^{19} cm^{-3} at the input facet. The same density drops to 10^{18} cm^{-3} and to 2×10^{17} cm^{-3} at L=2 mm and at L=10 mm, respectively. As a result, the largest compression occurs within the first ~2 mm due to FCA dominance, and then TPA induced pulse broadening dominate in the following ~8 mm waveguide segment. Hence, for 100 ps input pulses, the waveguides as short as 2 mm can provide more effective pulse compression with only 50% of peak power values used in 1cm. These results indicate that effective utilization of TPA and FCA requires optimization of the waveguide geometry for desired pulse parameters.

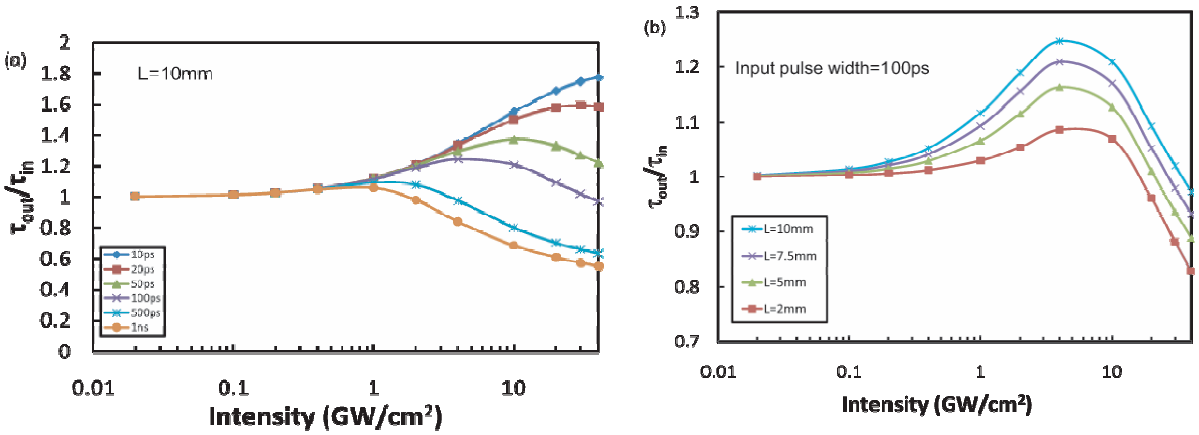

Fig. 4. Predicted pulse compression ratio in (a) 10 mm long silicon waveguide for different initial pulse widths and (b) silicon waveguides with different lengths.

3. EXPERIMENTAL RESULTS

3.1 Laser modelocking and pulse compression

Modelocking experiment of the pulse compression in silicon is demonstrated in a laser cavity formed by an erbium doped fiber amplifier (EDFA) gain medium, a silicon pulse compressor and a spool of standard fiber as illustrated in Fig. 5. The silicon waveguide used for pulse compression is a 1.7cm long silicon on insulator waveguide with ~5μm^2 effective area. The total fiber-to-fiber loss of the waveguide is measured to be ~2dB. The output of the waveguide is connected to a 10/90 tap coupler where 10% used as an output and 90% is fed into the gain medium, a high power

EDFA with 200 mW saturated output power. The resonator is formed by launching the EDFA output back into the silicon waveguide input. Since the pulse shaping by free carriers requires a time-dependent optical signal circulating inside the cavity, an 8 ns pulsed current source is connected to the waveguide to start initial pulsation at the fundamental cavity frequency of ~1.4MHz. The output pulse width is expected to be minimized when the frequency of the function generator matches the fundamental cavity frequency. Here, manual frequency locking is achieved by monitoring the pulse shape and the modulation frequency, simultaneously. The output of the resonator is connected to an optical spectrum analyzer and a photodetector followed by a 25GHz sampling oscilloscope or an RF spectrum analyzer to measure output characteristics. Since the pulse compression is intensity square dependent, at constant pulse width, the variation of rise and fall time can be used to tune the pulse energy and hence the number of free carriers generated by an optical pulse at fixed peak power.

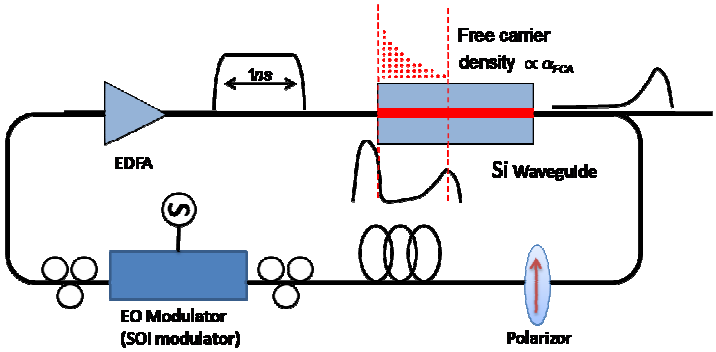

Fig. 5. Experimental setup used for TPA based modelocking and pulse compression scheme. SOI: Silicon on insulator waveguide, EDFA: erbium doped fiber amplifier

First, we confirm that the free carriers indeed help pulse compression by using 8 ns electronic modulation with rectangular pulse shape. By adjusting the gain of EDFA we control the peak power circulating inside the cavity. We observe that at low powers (<1mW at the output), the circulating signal is quite similar to the modulation signal, (Fig. 6).When we increase the gain of the EDFA to obtain 2mW at the output, we observe short pulse formation at the front edge of the pulse, as expected. Also, the experimental results show that most of the energy is contained under broad pedestal at these power levels and only a small portion of the energy is used for short pulse formation. However, as the power levels increase, the long pedestal is suppressed further down. These results indicate that this modelocking scheme will operate best at high intensities and will be limited by the broad pedestal at low intensity values.

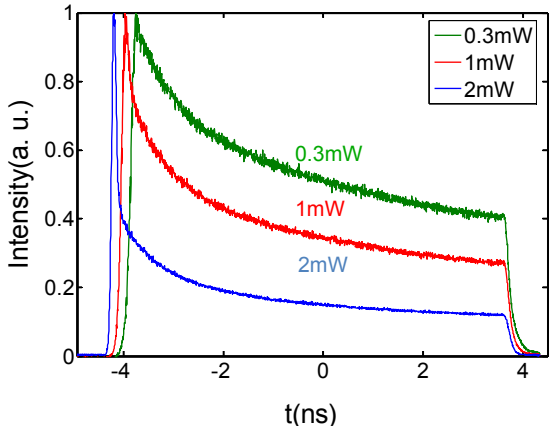

Fig. 6. Pulse compression results inside the laser cavity. Power values are measured at the output of the cavity.

Fig. 7(a) illustrates the pulse widths measured at the laser output for different peak powers and different rise/fall times. The shortest pulse width is measured to be 60 ps by using RF signals with 140ps rise/fall time. Fig. 4(b) shows the tendency of the pulse compression with respect to different peak powers and different rise/fall times. At fixed pulse energy, slower rise time results in fewer free carrier generation. As a result, the pulse width increases to 85ps if the rise time is tuned to 650ps for the same pulse energy. These measurements indicate that free carrier concentration increases more rapidly for modulation signals with sharper rise times. To compensate the slope effect we need to increase pulse energy to achieve the same compression, as shown in Fig. 7(b). This tendency agrees with the theoretical results presented in Fig. 4(a), which shows the higher peak power requirement for low energy pulses. For instance, to achieve 80 ps output pulses, the average power entering the silicon waveguide has to be maintained at 9dBm, 13dBm and 16dBm levels for 140 ps, 450 ps and 650 ps rise and fall times, respectively. The peak power corresponding to 80ps pulse with 9 dBm average power is ~120 W (2.4G W/cm^2). The total loss at this setting is measured to be <6dB, of which 2dB is the linear loss and the rest originates from the nonlinear effects.

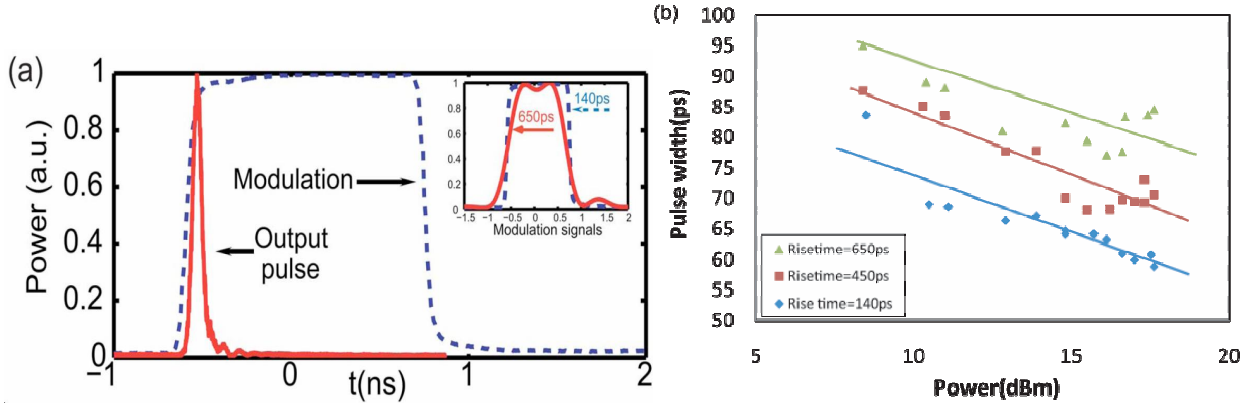

Fig. 7. (a) Laser output and the 1.5 ns modulation with 140 ps rise time. (Inset) Modulation signals used for modelocking experiment. (b) Variation of output pulse width with respect to pulse energy.

3.2 Raman amplification using compressed pulses

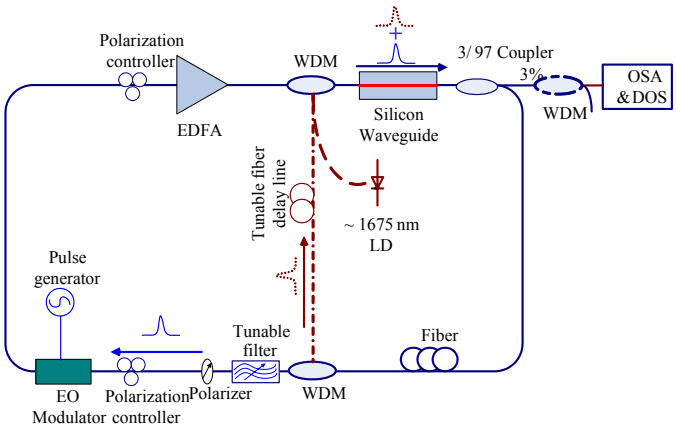

Fig. 8. Experimental setup for testing Raman amplification and dual wavelength lasing

Net gain amplification and lasing in silicon have been previously demonstrated using a pulsed-pumping technique [1,3]. To study stimulated Raman scattering inside the modelocked laser cavity, a simple pump-probe experiment is conducted by using a continuous wave (CW) probe laser around 1675 nm. The setup is shown in Fig. 8. In this experiment, Raman gain inside the laser cavity is measured for various pulsing conditions. We show that a 2.8 dB Raman gain can be measured at the front end of a long pulse with a large pedestal when the modelocking condition is

not optimized, as shown in Fig 9. However, at the same time, the pulse suffers from a 7 dB free carrier loss at the trailing edge. Hence, for low loss and an effective Raman effect, the fundamental pulse modelocking should be optimized before the Raman cavity is formed.

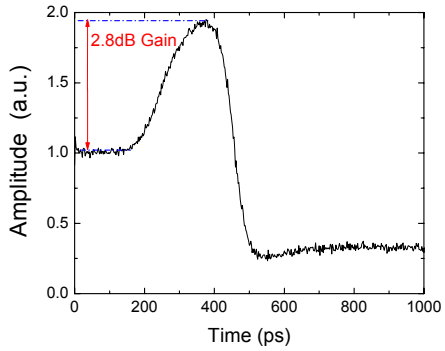

Fig.9. Raman gain pumped with compressed pulses

3.3 Dual wavelength short pulses lasing

The observation of a 2.8 dB gain indicates that a careful design of the laser cavity can facilitate lasing at the Stokes wavelength by stimulated Raman scattering without an additional pump and hence enhance the functionality of the silicon chip [21]. Because of wavelength selectivity of the filter, another cavity for Raman Stokes pulse is needed. To facilitate resonance at the pump wavelength and the Stokes wavelength, the experimental setup is modified according to dashed line in Fig. 8. After removing the probe CW laser, the original laser cavity is modified by using two WDM couplers, which separate the Stokes from the wavelength sensitive components in the pulse compression cavity and recombine before the silicon waveguide, and a tunable fiber delay. Once modelocking is optimized to generate short pulses, we are able to utilize the short pulses as the pump to achieve stimulated Raman scattering and modelocking in the second cavity. After pulses at both wavelengths are aligned temporally, we observe lasing at Stokes and pump wavelengths. The spectra of the dual wavelength laser are shown in Fig. 10. The pump wavelength is selected by the band pass filter inside the laser cavity to be 1540 nm and the expected Raman Stokes signal is at wavelength of 1675 nm [3].

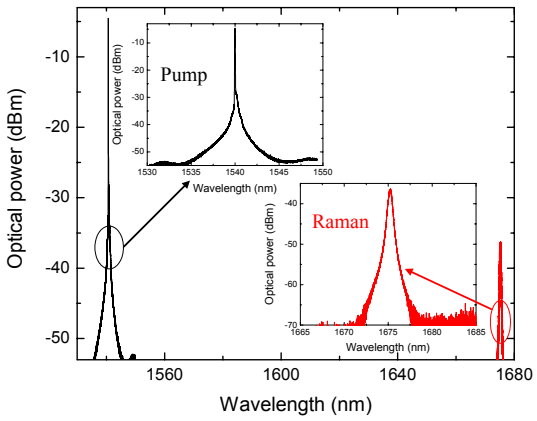

Fig.10. Spectra of the pulse-compressed pump and Raman laser

Fig. 11(a) illustrates the 100 ps mode-locked pulses generated inside the main laser cavity. Due to the polarization sensitivity of the modelocking and Raman processes, we observe that the fundamental pulse width is slightly broader than pure modelocking optimum and it is difficult to simultaneously achieve modelocking and Raman lasing. Fig. 11(b) shows the Raman Stokes pulse observed at the output. Since free carriers are created and accumulate in the silicon waveguide, the Raman Stokes pulse also suffers from free carrier attenuation. Therefore, the final outcome of the Raman Stokes pulses is the combination of Raman amplification, TPA, and free carrier effect. To measure the lasing threshold at the Stokes wavelength, we change the pump power circulating inside the laser cavity. Fig. 12 illustrates the variation in Stokes power with respect to EDFA output power sweep from 0 to 6 mW. The lasing threshold is measured to be ~3.75 mW [21]. Since the pump pulse width is a function of EDFA output power, we observe different Stokes pulse widths at different EDFA output power levels. Increasing the EDFA output power above 5 mW causes the Raman output power to enter into saturation because of nonlinear losses including TPA and FCA.

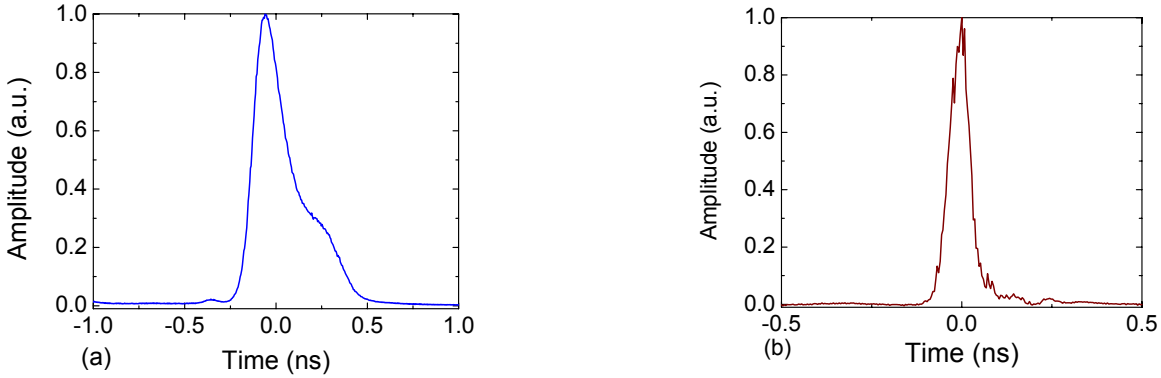

Fig.11. Time profiles for (a) the compressed pump and (b) Raman pulses

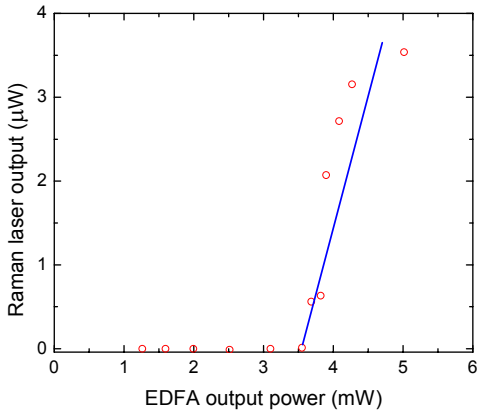

Fig.12. Raman laser output power as a function of EDFA output power.

4. CONCLUSION

The transient behavior of free carrier concentration has prominent effects on silicon based ultrafast applications. For free carrier plasma effect, this manifests itself just as a scaling of index change. However, for FCA and TPA based pulse shaping devices, aggregate response will differ based on their operation in TPA dominate regime and FCA dominant regime. For pulse compression and modelocking, we need TPA dominant regime at the front end of the pulse and FCA dominance at the trailing edge. We experimentally demonstrate pulse compression and modelocking scheme by utilizing

TPA and FCA in silicon waveguides. We also demonstrate that the generated short pulse can also act as a pump for stimulated Raman scattering in the same silicon chip and provide dual wavelength lasing. Laser modelocking and dual wavelength lasing at 1540 nm and 1675 nm are experimentally achieved using a silicon waveguide in the dual-fiber-ring-cavity with an EDFA and silicon as the gain media. The performance of pulse compression in the silicon waveguide can be enhanced using small core waveguides [12, 13-14], which can stimulate the Raman effect at even lower powers. Additionally, the broadband nature of this modelocking scheme may deliver short pulses and facilitate nonlinear optical devices at wavelengths where conventional saturable absorber modelocking fails.

REFERENCE

[1] L. Ansheng, R. Haisheng, R. Jones *et al.*, "Optical amplification and lasing by stimulated Raman scattering in silicon waveguides," Journal of Lightwave Technology 24(3), 1440 (2006).

[2] O. Boyraz, and B. Jalali, "Demonstration of 11dB fiber-to-fiber gain in a silicon Raman amplifier," IEICE Electronics Express 1(14), 429 (2004).

[3] O. Boyraz, and B. Jalali, "Demonstration of a silicon Raman laser," Optics Express 12(21), 5269 (2004).

[4] H. Rong, A. Liu, R. Jones *et al.*, "An all-silicon Raman laser," Nature 433(7023), 292-294 (2005).

[5] A. Liu, R. Jones, L. Liao *et al.*, "A high-speed silicon optical modulator based on a metal-oxide-semiconductor capacitor," Nature 427(6975), 615-618 (2004).

[6] A. Liu, L. Liao, D. Rubin *et al.*, "High-speed optical modulation based on carrier depletion in a silicon waveguide," Optics Express 15(2), 660-668 (2007).

[7] V. Raghunathan, R. Claps, D. Dimitropoulos *et al.*, "Parametric Raman wavelength conversion in scaled silicon waveguides," Journal of Lightwave Technology 23(6), 2094-2102 (2005).

[8] K. Yamada, H. Fukuda, T. Tsuchizawa *et al.*, "All-optical efficient wavelength conversion using silicon photonic wire waveguide," IEEE Photonics Technology Letters 18(9), 1046-1048 (2006).

[9] K. K. Tsia, S. Fathpour, and B. Jalali, "Energy harvesting in silicon wavelength converters," Optics Express 14(25), 12327-12333 (2006).

[10] Boyraz, P. Koonath, V. Raghunathan *et al.*, "All optical switching and continuum generation in silicon waveguides," Optics Express 12(17), 4094-4102 (2004).

[11] V. R. Almeida, C. A. Barrios, R. R. Panepucci *et al.*, "All-optical control of light on a silicon chip," Nature 431(7012), 1081-1084 (2004).

[12] V. R. Almeida, C. A. Barrios, R. R. Panepucci *et al.*, "All-optical switching on a silicon chip," Optics Letters 29(24), 2867-2869 (2004).

[13] E. K. Tien, N. S. Yuksek, F. Qian *et al.*, "Pulse compression and modelocking by using TPA in silicon waveguides," Optics Express 15(10), 6500-6506 (2007).

[14] E. K. Tien, F. Qian, N. S. Yuksek *et al.*, "Influence of nonlinear loss competition on pulse compression and nonlinear optics in silicon," Applied Physics Letters 91, 201115 (2007).

[15] Y. Okawachi, M. Foster, J. Sharping *et al.*, "All-optical slow-light on a photonic chip," Optics Express 14(6), 2317-2322 (2006).

[16] F. Xia, L. Sekaric, and Y. Vlasov, "Ultracompact optical buffers on a silicon chip," Nature Photonics 1(1), 65 (2007).

[17] T. Liang, L. Nunes, T. Sakamoto *et al.*, "Ultrafast all-optical switching by cross-absorption modulation in silicon wire waveguides," Optics Express 13(19), 7298-7303 (2005).

[18] T. K. Liang, H. K. Tsang, I. E. Day *et al.*, "Silicon waveguide two-photon absorption detector at 1.5 μm wavelength for autocorrelation measurements," Applied Physics Letters 81, 1323 (2002).

[19] R. Dekker, A. Driessen, T. Wahlbrink *et al.*, "Ultrafast Kerr-induced all-optical wavelength conversion in silicon waveguides using 1.55 μm femtosecond pulses," Optics Express 14(18), 8336-8346 (2006).

[20] M. J. Kerr, and A. Cuevas, "General parameterization of Auger recombination in crystalline silicon," Journal of Applied Physics 91, 2473 (2002).

[21] X. Sang, E.-K.Tien, N. S. Yuksek *et al.*, "Dual-wavelength mode-locked fiber laser with an intracavity silicon waveguide," IEEE Photonics Technology Letter 20, 1184-1186 (2008).